Supporting Information

Classification of crystal structures of thiophene-containing organic semiconductors

Takehiko Mori

Department of Materials Science and Engineering, Tokyo Institute of Technology, O-okayama 2-12-1, Meguro-ku, Tokyo 152-8552, Japan. E-mail: mori.t@mac.titech.ac.jp

Parameters of intermolecular interaction

The intermolecular energy was estimated according to the standard 6-exp potential,[S1-S8]

$$V = \varepsilon\left[A\exp(-B\frac{r}{r_0}) - C(\frac{r_0}{r})^6 \right] + D\rho_i\rho_j / r_0 \qquad \text{(S1)}$$

where A = 184000, B = 12, C = 2.25, and D = 1380 kJ Å mol^{-1}.[S9] The parameters were taken from the MM3 force field (Table S1).[7,29,S10] The dispersion represented by this equation has a minimum of 1.12ε at r_0. For interaction between different atoms, the geometrical average was used for ε, while the arithmetic average was used for r_0. There were no reliable parameters for Se, but the values that gave slightly larger potentials than S were used. To this dispersion energy, electrostatic energy coming from the last term was added.[S3-S5,S8] Charges ρ_i calculated from the molecular orbitals scattered largely,[7] and significantly depended on the estimation methods, hence the same charge was allotted to the same kind of atoms (Table S1). The opposite charge was allotted to the connecting carbon atoms so as to maintain the charge neutrality (Fig. S1(b)). Charges on N and S were either positive or negative depending on the environments, so the average values were adopted. The results reproduced the reported charges well.[7] Usually, electrostatic energy between various atoms canceled each other, and the total electrostatic contribution was 5-6% of the total intermolecular energy (Fig. S12-S15).

Table S1 Force-field parameters[S11]

Atom	ε (kJ mol^{-1})	r_0 (Å)	Charge ρ_i
C	0.2343	3.92	–
H	0.0837	3.24	0.115
S	0.8452	4.30	0.07
O	0.2466	3.64	−0.30
N	0.1797	3.86	0.00
Se	1.8	4.30	0.07

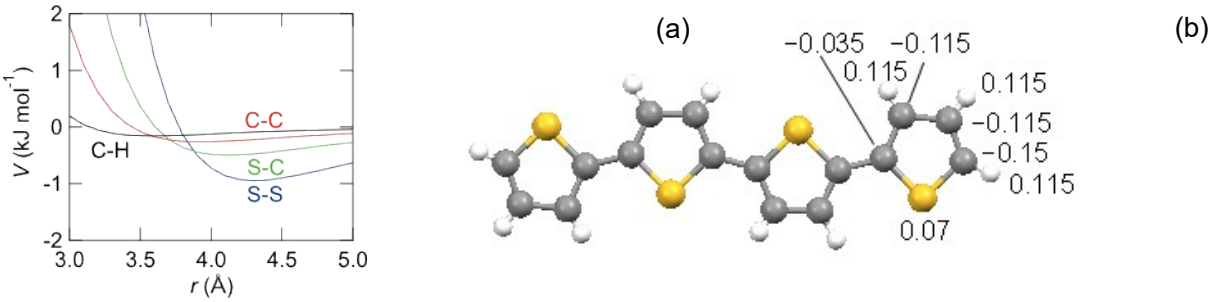

Fig. S1 (a) Potential curves based on eq (S1) and Table S1. (b) Charges on 4T.

W and L are related to m in fused molecules (Fig. S2).

$$W = 1.66 + 2.46m \quad \text{(S2)}$$

However, W of acenes, typically 4.8 Å is slightly larger than those of nP (4.2 Å, Table 1), and those of fused TTT molecules (< 4.0 Å, Table 2) are slightly smaller than those of the ordinary HB molecules (Table 1). Molecules including an odd number of thiophene rings have a V-shape, and the entries after PPTPP in Table 1 have large W > 5.3 Å.[69-76] Despite the large W, all these one-leg molecules have HB structures, but tend to have small θ around 40° in order to adjust the large W to the HB structure.

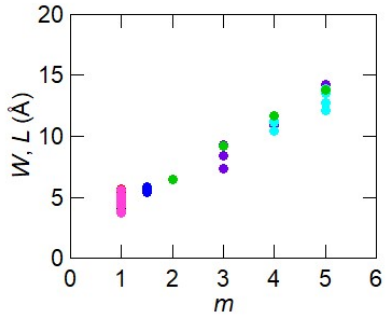

Fig. S2 W and L as a function of the leg number m.

Other structure parameters of HB structures

Coordinates (X_g', Y_g', Z_g') of the center of the bottom molecule represented by the molecular coordinates of the top molecule (Fig. 1(a)) are listed in Table S2 and S3. Similar to eqn 4, Y_g' and Z_g' are evaluated from a, b, and θ.

$$Y_g' = \frac{a}{2}\sin\frac{\theta}{2} + \frac{b}{2}\cos\frac{\theta}{2}$$

$$Z_g' = \frac{a}{2}\cos\frac{\theta}{2} - \frac{b}{2}\sin\frac{\theta}{2} \qquad \text{(S3)}$$

In analogy with Fig. 4(b), these relations reproduce the actual values taken from Table S2 and S3 satisfactorily (Fig. S3).

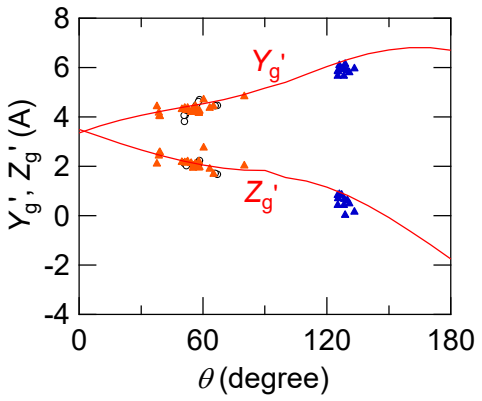

Fig. S3 Y_g' and Z_g 'as a function of θ estimated from eqn (S3).

When molecular coordinates of respective atoms of the bottom molecule (X, Y, Z) are given, coordinates of the top molecule are obtained.

$$X' = -X + X_g$$

$$Y' = Y\cos\theta + Z\sin\theta + Y_g$$

$$Z' = Y\sin\theta - Z\cos\theta + Z_g \qquad \text{(S4)}$$

In thiophene-containing V-shaped molecules, the g molecule is generated by a screw axis instead of a glide plane. In such a case, the sign of Y' is inverted.

Table S2 Supplementary structure parameters of representative HB structures

Compound	L (Å)	X_g' (Å)	Y_g' (Å)	Z_g' (Å)	V_g (kJ mol^{-1})	V_X (kJ mol^{-1})	CCDC	
naphthalene	6.45	2.52	3.82	2.12	−15.76	−5.56/−4.12	1216814	30
anthracene	9.16	2.49	4.07	2.14	−23.16	−6.50/−3.62	1103062	31
tetracene*	11.67	2.02	4.20	2.17	−31.76	−4.39/−3.87	1502159	32
pentacene*	13.82	2.19	4.27	2.03	−39.19	−5.67/−2.30	619981	33
2P	9.14	1.23	4.48	1.67	−20.81	−7.18/−3.76	1111363	34
3P	13.50	1.21	4.47	1.68	−34.38	−3.39/−1.03	1269381	35
4P	18.07	1.22	4.46	1.72	−46.37	−7.68/−2.87	1245768	36
4T (high *T*)	15.73	2.50	4.23	2.03	−38.52	−5.98/−4.01	117770	37
6T (high *T*)	23.72	2.59	4.26	2.03	−62.42	−4.65/−3.54	1309241	38
8T	31.58	1.20	4.37	1.90	−80.17	−1.92/−0.84	1269355	39
6O	21.32	2.21	4.16	2.19	−40.64	−8.49/−2.09	750302	40
PTP	8.84	5.53	4.37	1.75	−11.68	−3.49/−3.38	257584	41
	s	4.22	1.49	3.48	−23.32			
TPT	8.55	0.42	4.30	2.10	−21.05	−6.83/−1.96	295043	42
TPPT[a]	11.25	1.78	4.18	2.12	−30.30	−3.00/−2.54	1899660	43
TPPPT	13.75	1.86	4.17	2.10	−39.13	−7.74/−3.75	944975	44
TPPPPT'	13.80	1.25	4.60	2.10	−43.58	−4.06	1544287	45
PTPTP	13.11	5.39	4.47	1.84	−26.96	−23.00/−5.43	667690	46
PTTP (BTBT)	10.74	0.49	4.44	2.11	−26.66	−5.90/−4.73	975935	47
PPTTPP (DNTT)	15.32	0.79	4.31	2.19	−45.50	−5.91/−4.51	644240	48
PPPTTPPP (DATT)	20.15	0.41	4.31	2.17	−63.67	−6.45/−4.95	839976	49
P-PTTP-P	19.05	0.07	4.29	2.35	−55.18	−4.56	837916	50
PSeSeP	10.68	0.68	4.72	2.02	−27.21	−3.37/−2.61	607975	51
P-PSeSeP-P	19.24	3.17	4.18	2.23	−50.80	−7.06/−4.58	607976	51
PTTPPTTP	19.23	0.34	4.36	2.20	−54.19	−5.30/−5.18	1001008	52
P-TPPT-P	19.96	0.84	4.30	2.00	−56.37	−6.25/−4.96	837914	50
T-TT-T	14.04	3.04	4.17	1.86	−30.68	−6.95/−3.91	625219	53
TT-TT	12.47	0.83	4.27	1.91	−26.77	−4.84/−3.99	625220	53
2P-TT-2P	23.66	1.24	4.43	1.69	−66.09	−7.08/−4.11	289196	54
PAP	8.85	0.23	4.55	1.60	−16.15	−3.02/−1.30	148755	55
PAPP	11.48	2.12	4.12	2.03	−23.93	−5.15/−3.83	696054	56
PPAPP	13.76	2.11	4.23	1.95	−39.96	−6.36/−2.77	220864	57
POP	8.63	0.00	4.47	2.01	−21.78	−4.46/−3.87	1137351	58
PNP	8.47	2.77	4.45	1.99	−20.73	−5.71/−4.20	1131619	59
PNNP	10.48	1.88	4.22	1.96	−20.11	−5.31/−3.48	1456637	18
P-NPN-P	17.09	0.99	4.17	1.95	−43.35	−4.94/−2.89	694651	60
PNPPNP	14.48	1.78	4.83	2.02	−29.05	−6.20/−4.20	1522122	61
phenanthrene	9.20	1.13	4.70	2.23	−17.98	−3.15	1232377	62
crysene	11.28	1.45	4.49	2.05	−29.80	−7.60/−4.74	1483901	63
picene	13.48	1.18	4.62	2.05	−36.65	−3.19	1319885	64
2P-2T-2P	25.28	1.01	4.36	2.02	−70.45	−6.60/−3.99	232983	65
2P-3T-2P	28.82	1.98	4.03	2.57	−79.29	−9.08/−3.72	232984	66
2P-4T-2P	32.98	1.31	4.27	2.14	−93.32	−3.60/−1.11	232985	66
2T-2P-2T	24.17	1.72	4.17	2.43	−65.46	−7.96/−1.69	619631	67
P-2O-P	15.38	0.07	4.47	2.04	−35.34	−5.83/−4.17	1585923	68
PPTPP	13.24	1.04	4.34	2.35	−40.59	−4.89	886147	69
PPTPP'	12.61	0.00	4.56	2.31	−40.58	−4.96/−4.27	898433	70
PPNPP	13.32	1.53	4.15	2.26	−36.81	−6.80/−3.67	1868302	71
PPPTPPP	17.77	1.05	4.15	2.70	−58.26	−2.93/−1.84	918807	72
PPPOPPP	17.98	0.56	4.09	2.43	−57.97	−8.29/−2.98	918806	72
PTTTP	12.68	0.00	4.58	2.04	−31.64	−6.10/−4.76	600120	73
P-TTT-P	16.44	0.04	4.04	2.54	−46.76	−6.19/−1.84	1005154	74
P-TTT-TTT-P	27.20	0.52	4.08	2.47	−71.39	−6.06/−5.13	1005153	75
P-PTTPPTTP-P	27.21	0.42	4.28	2.29	−82.50	−7.04/−4.50	1437639	76

Table S3 Supplementary structure parameters of representative θ-structures

Compound	*m*	*L* (Å)	X_g (Å)	Y_g (Å)	Z_g (Å)	V_g (kJ mol^{-1})	V_X (kJ mol^{-1})	CCDC	
TTT	1	8.21	2.05	5.66	0.43	−7.58	−4.05/−3.46	1025419	77
TTTT		10.12	6.78	5.66	0.63	−8.04	−4.06/−3.17	1189330	78
TTTTT		12.09	0.00	5.88	0.62	−13.73	−4.26	280212	79
TTT-TTT		15.85	0.78	5.81	0.50	−17.39	−5.51/−4.17	121235	80
T-TTT-T		15.79	0.00	5.96	0.16	−19.62	−5.28/−0.52	258755	81
PTTTTTP		16.62	0.00	5.94	0.84	−18.29	−4.22/−0.34	630757	82
PTPTP		13.13	5.20	5.86	0.83	−16.50	−10.80/−3.60	668464	83
PTTPTTP		16.97	0.58	6.09	0.87	−24.36	−4.44/−3.80	911947	84
PPTPTPP		17.62	8.27	5.79	0.80	−20.53	−18.30/−3.64	980613	85
PTT-TTP		16.58	5.07	5.85	0.70	−22.96	−11.13/−3.59	911203	86
PTTT-TTTP		20.43	0.75	5.93	0.68	−28.14	−4.58/−3.99	916021	87
PPSePP		13.33	7.48	5.16	1.60	−15.11	−3.00	2003835	88
DBTTF		12.62	4.40	6.14	0.03	−14.34	−7.58/−5.36	1426210	89
BTTTF		11.19	1.45	5.59	0.58	−16.25	−3.01/−2.15	1236389	90
dithiapyrene	2	8.21	6.08	4.96	2.13	−10.71	−4.65	1144889	91
TO-OT	1	11.81	2.37	5.37	0.36	−12.01	−2.55	1180370	92

Table S4 Structure parameters of representative γ-structures

Compound	*m*	X_g (Å)	Y_g (Å)	Z_g (Å)	V_g (kJ mol^{-1})	X_s (Å)	Y_s (Å)	Z_s (Å)	V_s (kJ mol^{-1})	V_X (kJ mol^{-1})	CCDC	Ref
coronene	3	4.32	0.36	7.19	−11.56	3.18	0.22	3.46	−60.06	−12.77/−3.07	1129883	93
ovalene	4	5.45	1.26	8.31	−12.94	2.93	1.26	3.45	−91.62	−19.21/−6.45	1226289	94
[18]annulene	3	0.37	3.10	7.17	−12.39	0.11	3.61	3.16	−49.87	−10.75/−6.69	1103169	95
kekulene	5	3.28	5.98	9.34	−18.10	1.97	2.41	3.36	−154.8	−19.13/−7.08	1194780	96
dithiaperylene	3	5.19	1.19	6.96	−11.52	2.72	0.11	3.42	−62.03	−6.64/−5.23	840103	97
dibenzoperylene	3	4.58	0.27	7.34	−21.85	2.27	3.27	3.40	−63.63	−23.49/−5.80	1137285	98
benzopyrene	4	6.77	2.19	7.57	−5.39	2.81	0.69	3.50	−50.11	−19.96/−4.11	1112703	94,S11

Table S5 Supplementary structure parameters of representative stacking structures

Compound	L (Å)	X_g (Å)	Y_g (Å)	Z_g (Å)	V_Y (kJ mol^{-1})	X_g (Å)	Y_g (Å)	Z_g (Å)	V_X (kJ mol^{-1})	CCDC	
Type I											
YZPP	11.17	4.75	6.33	0.73	−7.81	12.07	1.87	2.26	−6.29	2103754	99
PPQPP	13.92	3.85	7.11	1.19	−13.6	13.99	2.80	0.46	−2.68	1230895	100
PQPQP	13.89	10.97	4.92	2.69	−11.48	8.50	7.07	0.69	−8.50	703585	101
ZPQPZ	13.55	8.02	6.19	0.52	−9.65	16.04	1.73	3.38	−1.32	829331	102
quinacridone α	13.91	0.11	6.88	0.49	−5.83	15.72	1.41	1.52	−4.79	620257	103
Type IIa											
TPTPT	12.70	0.00	7.18	0.68	−11.55	12.84	1.33	2.87	−4.43	254385	104
PZQZP	13.54	7.51	6.4	0.36	−11.02	8.97	5.51	0.06	−7.53	761663	102
quinacridone β	13.80	0.50	6.91	0.47	−8.22	14.68	3.69	0.44	−4.98	620258	103
Type IIb											
POOP	10.45	0.06	6.3	1.39	−12.21	6.77	1.68	4.27	−9.12	1840406	105
PPOPP	12.09	4.41	7.81	1.34	−5.28	6.17	0.06	8.23	−9.26	898431	72
PQP	9.23	6.37	5.90	1.43	−8.00	9.67	0.29	2.71	−3.34	1103147	106
ZAPPP	13.61	7.37	5.63	1.10	−8.04	7.06	0.00	5.27	−11.33	870772	107
PZPP	11.21	3.23	5.98	1.84	−13.24	9.09	0.63	0.97	−11.91	2103753	99
PSeP	8.89	1.32	6.21	1.64	−8.54	6.85	2.87	3.05	−6.74	693675	108
α-TTF	7.80	4.52	5.53	1.79	−4.25	9.07	0.10	2.06	−5.84	618630	109
thienoisoindigo	10.23	10.4	6.84	1.93	−2.21	7.77	1.36	4.14	−8.80	1524783	110
Type III											
TTPTT	12.31	2.62	5.99	6.19	−7.69	7.66	0.21	8.52	−6.10	1434834	111
4O	14.37					8.85	0.46	5.76	−8.04	750303	40
(PAP)(PZP)	8.81	5.63	4.69	4.37	−4.65	6.03	0.91	3.45	−10.73	148756	55
indigo	12.30	4.69	1.19	5.13	−9.98	4.69	1.19	5.13	−9.98	1180370	112
quinacridone γ	13.82	13.38	3.49	4.00	−3.69	11.65	2.85	7.42	−3.75	620259	103

Low-symmetry HB structures

Tetracene and pentacene have triclinic symmetry,[32,33] in which two crystallographically independent molecules are located on inversion centers. Accordingly, there are two independent g and s interactions (Table S6). The symmetry is lowered so as to realize nonzero X_s = 1.76 and 1.55 Å in tetracene and 1.64 and 1.45 Å in pentacene. This happens so as to make the molecules tilted not only along the *a* axis but also along the *b* axis (Fig. S4(b)). However, Y_g, Z_g, Y_s, and Z_s are practically the same, and fulfill eqns (4) and (5). It is noteworthy that eqns (4) and (5) are satisfied only by placing molecules on inversion centers located at the center and corner of the lattice even without the glide symmetry. In the thin-film phase,[S12-S14] pentacene X_s becomes 0.57 and 0.60 Å (Table S6). The molecules are close to the substrate normal, and are advantageous to the charge transport. The thin-film phase is close to the ordinary HB structure. Even in the thin films, Y_g, Z_g, Y_s, and Z_s are practically the same as the other cases (Table S6).

The high-temperature phase of 4T has the ordinary $P2_1/a$ symmetry,[37] but the low-temperature phase is doubled along the *c* axis and the molecules are located on a general position in keeping the monoclinic symmetry.[S15] This leads to two kinds of glide interactions (Table S6), and X_s changes from 0.18 to 2.63 Å. The nonzero X_s results in a more tilted structure characteristic of the low-temperature phase. 6T has a similar low-temperature phase, and the ordinary 8T phase corresponds to the low-temperature phase.[39] Although the manner of symmetry lowering is different, the less tilted high-temperature phase of 4T corresponds to the thin-film phase of pentacene.

Table S6 Structure parameters of low symmetry HB structures

Compound	a (Å)	b (Å)	θ (°)	W (Å)	X_g (Å)	Y_g (Å)	Z_g (Å)	V_g (kJ mol^{-1})	X_s (Å)	Y_s (Å)	Z_s (Å)	V_s (kJ mol^{-1})	CCDC	
tetracene	7.98	6.14	50.89	4.97	0.26	−1.06	4.80	−33.33	1.76	5.26	2.64	−25.19	1502159	32
					1.91	−1.02	4.67	−31.76	1.55	5.41	2.45	−24.31		
pentacene	8.058	6.119	53.39	4.69	0.38	−0.92	4.78	−38.07	1.64	5.25	2.67	−27.84	619981	33
				4.71	1.89	−0.64	4.79	−39.50	1.45	5.31	2.66	−27.54		
pentacene TF	8.058	6.119	53.39	4.68	0.35	−0.91	4.73	−40.34	0.57	5.28	2.70	−27.73	665900	S14
				4.68	0.20	−0.89	4.73	−40.46	0.60	5.27	2.72	−27.82		
4T (high T)	8.936	5.7504	55.31	4.96	2.31	−0.86	4.70	−38.52	0.18	5.09	2.67	−28.71	117770	37
4T (low T)	7.7741	6.0348	62.39	4.78	1.14	−0.27	4.74	−37.04	2.63	4.61	2.86	−29.47	1441400	S15
					1.31	−0.32	4.77	−37.28						
6T (high T)	9.1404	5.6843	56.04	4.58	2.52	−0.76	4.70	−62.42	0.08	5.02	2.67	−45.10	1309241	38
8T	7.842	6.002	63.28	4.77	1.16	−0.26	4.77	−78.78	2.46	4.65	2.88	−70.72	1269355	39
					1.26	−0.28	4.79	−80.17						
TPT	7.803	5.842	54.3	4.75	0.29	−0.69	4.72	−21.81	1.53	5.00	2.61	−14.57	295043	42
								−21.27	1.50	5.01	2.60	−16.86		
TPPT	7.8065	5.8903	52.6	4.72	0.29	−0.92	4.67	−29.89	1.49	5.10	2.55	−23.04	1899660	43
					0.15	−0.87	4.64	−32.52	1.44	5.13	2.52	−22.09		
TPPPT	7.772	5.9155	51.67	4.78	0.36	−0.96	4.62	−36.80	1.50	5.14	2.52	−29.61	944975	44
				4.75	1.80	−0.95	4.60	−36.34	1.43	5.17	2.49	−28.84		
PAPP	7.8508	5.8275	54.93	4.81	0.35	−0.78	4.63	−31.74	1.77	4.91	2.60	−25.74	696054	56
				4.65	0.29	−0.78	4.58	−33.67	1.57	5.00	2.54	−28.56		
PPAPP	8.853	5.7504	54.95	4.65	2.81	0.83	4.58	−38.23	0.69	5.07	2.63	−33.26	220864	57
				4.64	2.05	0.865	4.65	−38.15	0.80	5.05	-2.63	−33.52		

(a) 3P (b) Tetracene

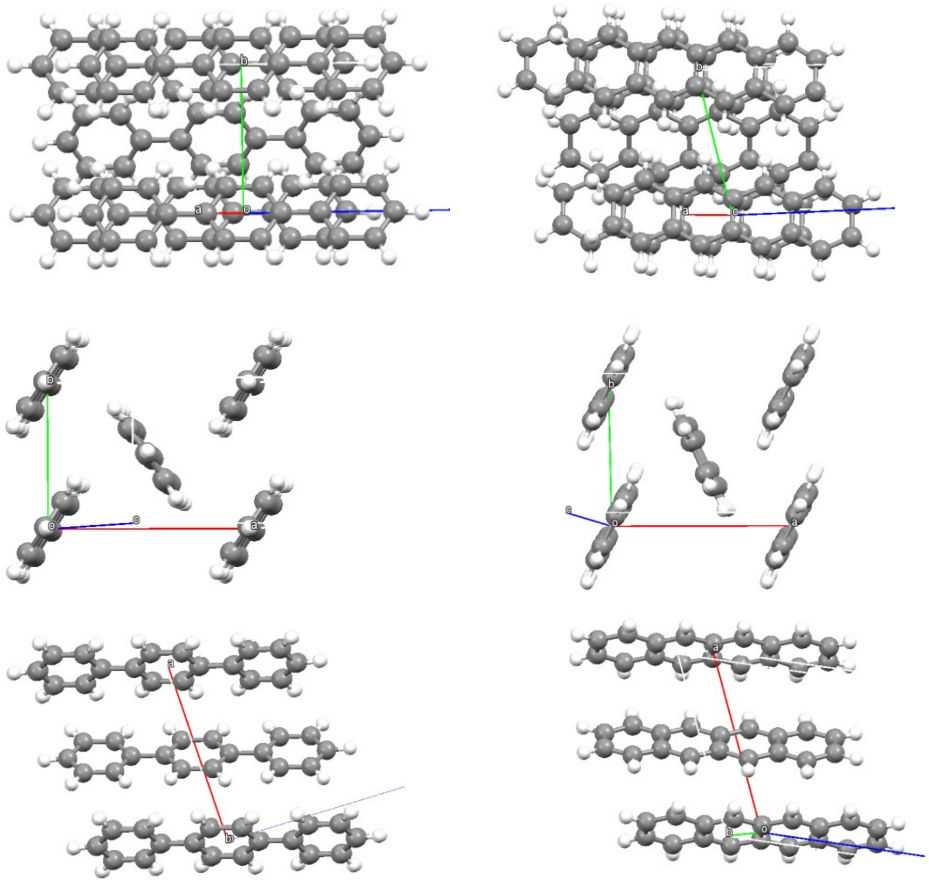

Fig. S4 Crystal structures of (a) 3P and (b) tetracene.

Lattice constants of HB structures

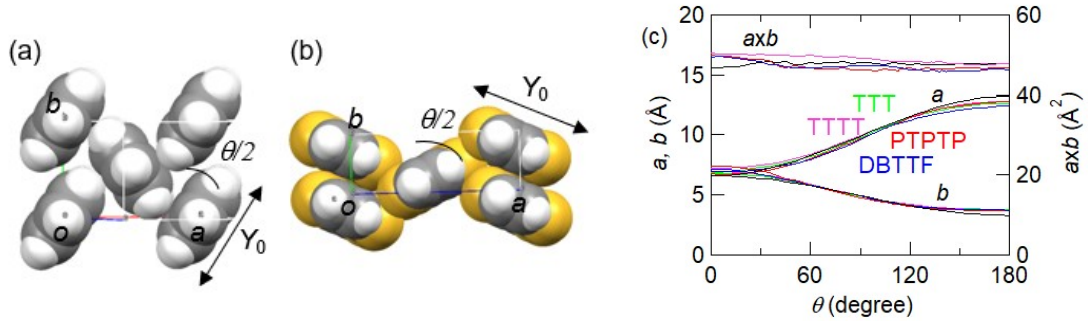

Fig. S5 Molecular contacts in the (a) HB, and (b) θ-structures. (c) Lattice constants *a* and *b* before (black) and after the optimization (colored) in θ-structure materials.

A molecule is assumed to be a plate with a thickness Z_0 and a width Y_0. Then, θ dependence of the lattice constants is derived from the condition of molecular contacts shown in Fig. S5(a) and (b).

$$a = 2Z_0 / \cos\frac{\theta}{2} \tag{S5}$$

$$b = Y_0 \cos\frac{\theta}{2} \quad \text{for HB} \tag{S6}$$

$$a = 2Y_0 \sin\frac{\theta}{2} \tag{S7}$$

$$b = Z_0 / \sin\frac{\theta}{2} \quad \text{for the θ- and γ-structures} \tag{S8}$$

Here Z_0 = 3.45 Å is the thickness of the molecule, and $Y_0 = W$ + 1.9 Å is used by adding the van der Waals radius of hydrogen to *W*. We have tried various parameters, but after optimization, the lattice constants in Fig. 4(a) and S5(c) are well represented by cosine functions in eqns (6) and (7). In the above equations, we have to smoothly connect the HB and θ-structure regions, but the cosine functions are smooth functions. It is noteworthy that the resulting $a \times b$ is almost θ independent (Fig. 4(a) and S5(c)), indicating that the lattice "volume" is constant due to the absence of redundant intermolecular space. In more than 1.5-leg compounds, this is not automatically satisfied, so

$$b = \frac{2Y_0Z_0}{a} \tag{S8}$$

is used instead of eqn (7). By this, Z_s is kept at Z_0 down to 60° even in the γ-structures.

Normalized potential curves

Fig. S6(a) demonstrates that V_g and V_s are scaled by N_{core}; intermolecular energy is in proportion to the molecular size. In particular, θ-structure and HB materials attain excellent linearity. However, γ-structure materials are scattered because this category includes molecules with various shapes. There is a linear relation in the form of $V = a\ N_{core} + b$, where the a and b values are listed in Table S7. Nonzero b is associated with nonzero X_g and X_s.

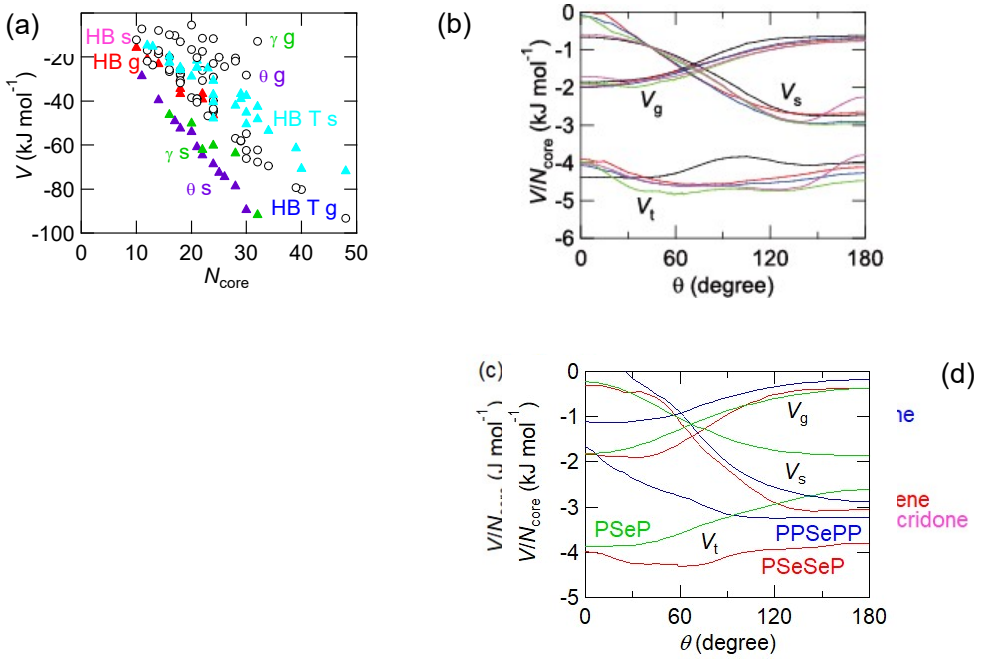

Fig. S6 (a) V_g and V_s as a function of N_{core} for HB acenes and nP (red/pink), HB nT and thienoacenes (blue/pale blue), θ-structures (purple), and γ-structures (green). (b) Potential curves of θ-structures using X_g = 0 Å. (c) Potential curves of stacking and SHB materials. (d) Potential curves of Se-containing materials.

Table S7 Linear parameters extracted from Fig. S6(a)

	g		s	
	a	*b*	*a*	*b*
HB	−2.05	4.84	−1.33	−0.99
θ	−1.10	6.17	−3.03	3.66
γ	−0.56	1.20	−2.56	−1.69

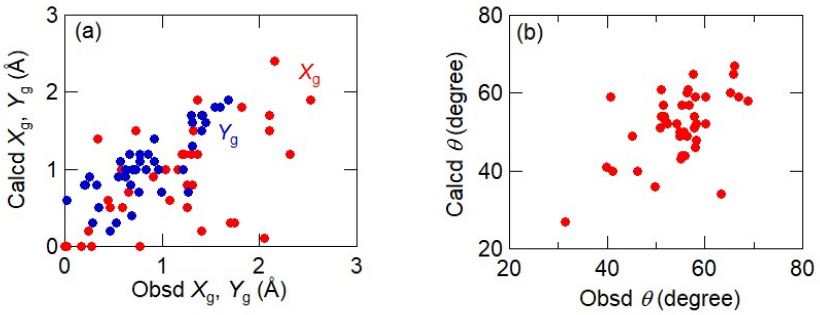

Fig. S7 (a) Relation of calculated X_g and Y_g obtained from the potential minimum (Fig. 3(a) and (b)) and the observed values. (b) Relation of calculated θ obtained from the potential minimum (Fig. 5) and the observed values.

Rotation of the γ-structures

In coronene, the original X axis (horizontal axis in Fig. S8(a)) has the zig-zag edge at the right and left edges. In analogy with the HB structures, the X axis defines L, and at $\varphi \sim 0^{o}$ the upper and lower armchair edges form the vertical contact edges (Fig. 7(c)). In contrast, $\varphi \sim 90^{o}$ (Fig. 7(b)) indicates that the zig-zag edge makes the contact edge. The latter is realized in the actual crystal. The potential is, however, a periodical function of 60^{o}.

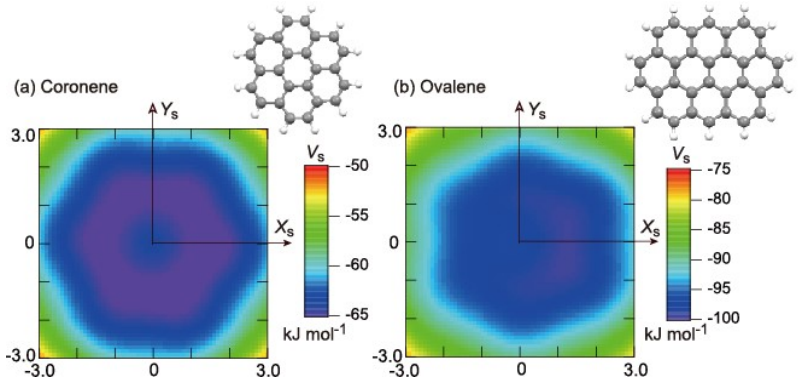

Fig. S8 Intermolecular energy of (a) coronene stack, and (b) ovalene stack as a function of X_s and Y_s (Å).

In Table S8, bold W or L is approximately perpendicular to the contact edge, which forms the zig-zag direction, and defines W^* used in eqn 6 to evaluate a. In some cases, molecular rotation φ within the molecular plane is necessary,

$$X_0^* = X_0 \cos^2 \phi + Y_0 \sin^2 \phi \quad \text{(S10)}$$

$$Y_0^* = X_0 \sin^2 \phi + Y_0 \cos^2 \phi \quad \text{(S11)}$$

where X_0 and Y_0 are L + 1.9 Å and W + 1.9 Å, respectively. Here, $\varphi = 0^{o}$ is defined by the direction with largest L. After this rotation, positions of the glide and stack molecules are estimated by using eqns 4-7, and the contact patterns shown in Fig. 7 are obtained. Here, L and W are rotated similarly. Following this procedure, we can investigate hypothetical patterns as shown in Table S9 and Fig. S9.

Table S8 Structure parameters of large-core γ-structures in the zig-zag direction.

Compound	*m*	*W*(Å)	*L* (Å)	*W** (Å) (φ)	*θ* (°)	Calcd *a* (Å)	Obsd *a* (Å)
coronene	3	9.23	**9.28**	9.28	94.77	16.52	16.119
ovalene	4	9.18	11.42	10.86 (120°)	94.34	18.86	19.47
dithiaperylene	3	7.33	**8.80**	8.80	102.9	16.89	15.436 (*a*+*c*)
dibenzoperylene	3	8.42	14.17	9.86 (150°)	81.01	15.41	16.98
benzopyrene	4	6.91	**11.19**	11.19	106.9	21.56	20.40

Table S9 Comparative stability of two patterns of γ-structure coronene, and the HB and stacking γ-structures in PTTP/POOP and PAPP/PZPP.

φ	Contact	*W*	V_g (V_{stat}) [e] (kJ mol^{-1})	V_s [e] (kJ mol^{-1})	V_{side} [e] (kJ mol^{-1})	V_t [e] (kJ mol^{-1})
coronene						
90°	Zig-zag	Armchair	−12.35	−58.01		**−82.80**
0°	Armchair	Zig-zag	−10.42	−57.69		−78.57
V(0°)−*V*(90°)			−1.93	−0.32		−4.23
	Structure	*W* (Å)				
PTTP (BTBT)	HB	4.69	−26.66	−19.55	−5.90/−4.73	**−88.23**
	Stacking [a]	10.74	−9.62	−28.57	−9.19/−4.59	−70.79
POOP	HB [b]	4.67	−22.55	−19.32	−4.69/−3.14	−75.39
	Stacking	10.45	−12.07	−33.29	−8.97/−4.59	**−79.96**
PAPP	HB		−34.21/−30.97	−28.56/−26.14	−4.28/−3.91	**−100.72**
			(−57.11/−60.17)	(−48.41/−46.80)		**(−164.89)**
	Stacking [c]		−12.12	−43.29/ −28.09	−11.92/−9.86	−81.71
			(−18.00/−10.19)	(−58.17/−40.86)	(−30.85)	(−134.31)
PZPP	HB [d]		−29.08/−26.06	−22.35	−5.14/−3.83	−86.46
			(−42.30/−45.60)	(−29.92/−28.81)		(−117.27)
	Stacking		−11.91	−43.14 /−27.70	−13.24/−12.52	**−85.00**
			(−19.76/−10.34)	(−64.42/−41.31)	(−23.18)	(**−124.16**)

[a] Oxygen atoms in the stacking (γ-structure) POOP are replaced by sulfur atoms. $V_t = 2V_g + V_s + 2V_{side}$

[b] Sulfur atoms in the HB PTTP are replaced by oxygen atoms. $V_t = 2V_g + V_s + \Sigma V_{side}$

[c] Hydrogen atoms are added to the stacking (γ-structure) PZPP. There are two crystallographically independent interactions similar to Table S6.

[d] Hydrogen atoms in the HB PAPP are removed. There are two crystallographically independent interactions similar to Table S6. $V_t = \Sigma V_g + (1/2)\,\Sigma V_s$

[e] BLYP-D3/TZP on ADF in the parentheses.[S16,S17]

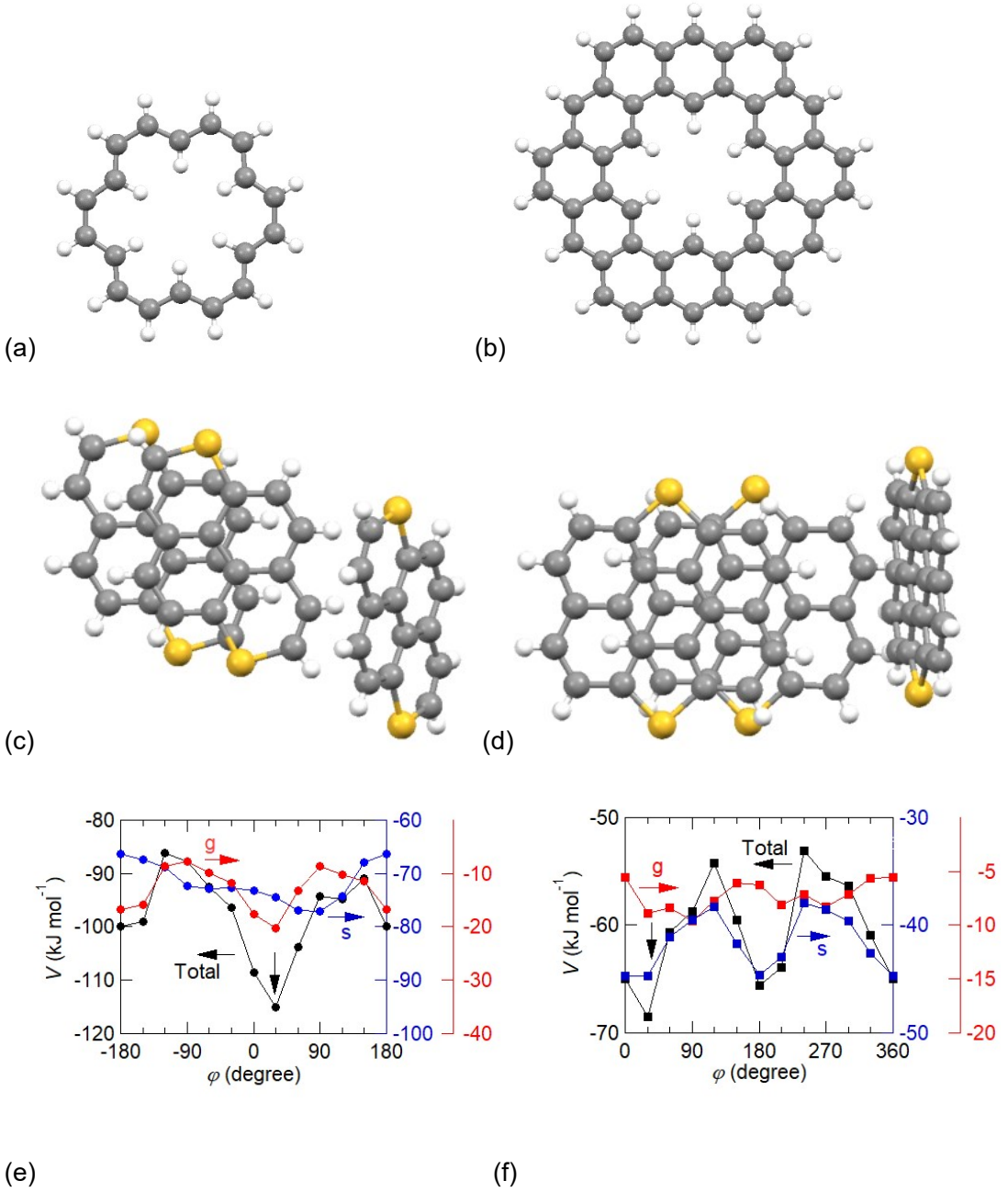

Fig. S9 Molecular structures of (a) [18]annulene, and (b) kekulene. Contact patterns of (c) dithiapyrene, and (d) dithiaperylene. Total energy $V_t = 2\ V_g + V_s$ of g-structure (e) dibenzoperylene, and (f) dithiapyrene molecules as a function the rotation angle φ within the molecular plane. The vertical arrows indicate the actual structures.

Stacking structures

(a) YZPP (Type I) (b) PQPQP (Type I)

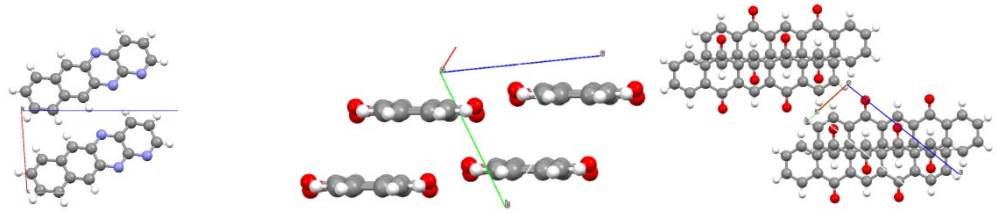

(c) Quinacridone β (Type IIa)

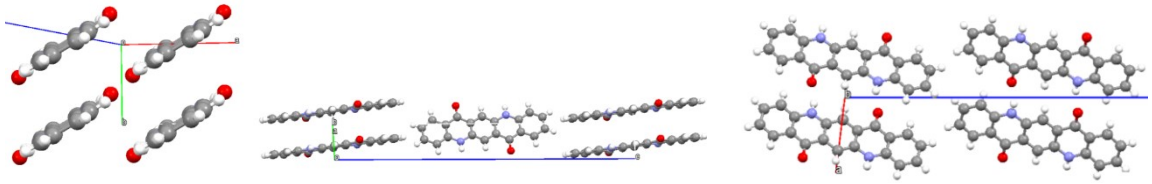

(d) POOP (Type IIb) (e) PZPP (Type IIb)

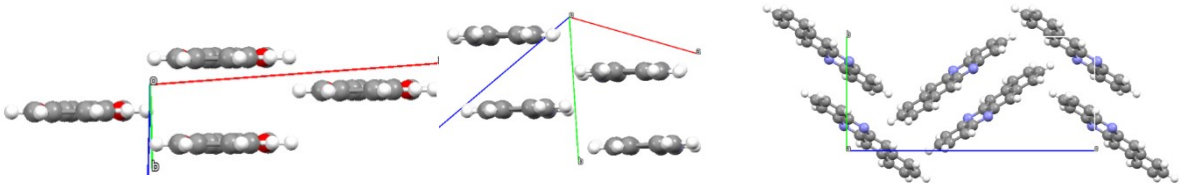

(f) TTPTT (Type III)

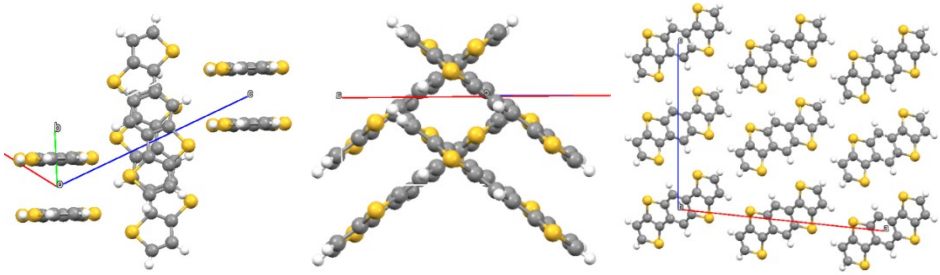

(g) (PAP)(PZP) (Type III) (h) Indigo (Type II)

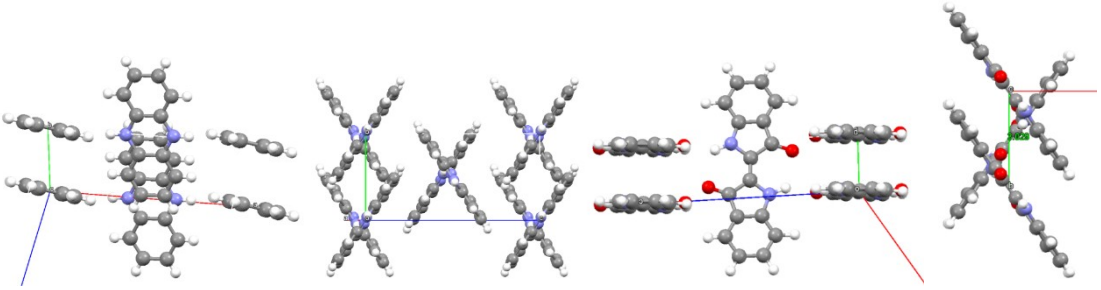

Fig. S10 Representative stacking structures of (a) YZPP (Type I), (b) PQPQP (Type I), (c) quinacridone β (Type IIa), (d) POOP (TypeIIb), (e) PZPP (Type IIb), (f) TTPTT (Type III), (g) (PAP)(PZP) (Type III), and (h) indigo (Type III).

S1 interaction in SHB

Fig. S11 is the intermolecular energy for s1 in pyrene and perylene at Z_s = 3.45 Å calculated using 6-exp and BLYP-D3.[S16,S17] For pyrene in 6-exp, (X_s, Y_s) = (0.0, 1.7) (Å) (−33.8 kJ mol^{-1}) is slightly lower than the second minimum at (1.7, 0.0) (−32.9 kJ mol^{-1}). By BLPY-D3, however, the minimum appears at (1.8, 0.0) in agreement with the actual crystal structure (1.78, 0.10). In perylene, both 6-exp (1.4, 1.3) and BLYP-D3 (1.0, 1.5) reproduce the actual geometry (1.11, 1.36). Accordingly, the s1 geometry in the SHB structures is regarded as the optimal stacking geometry.

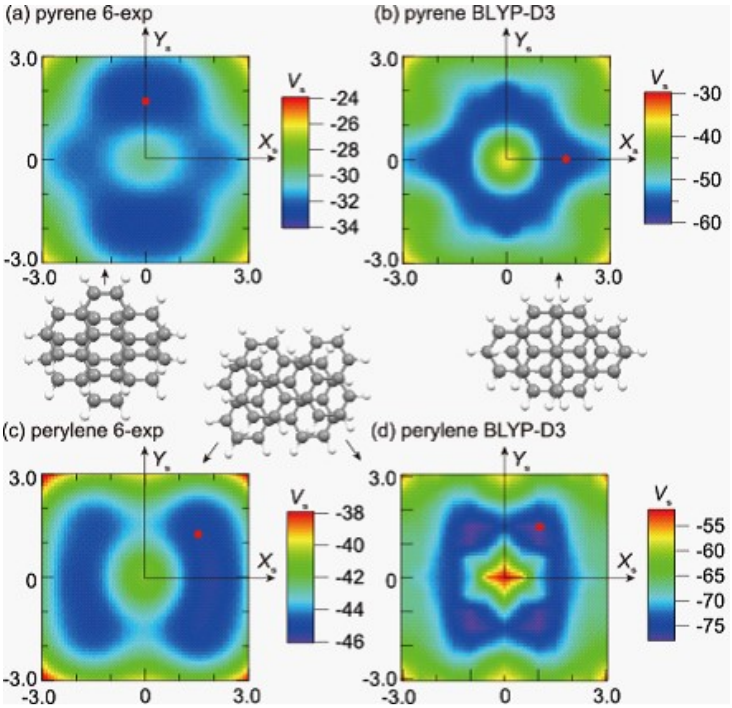

Fig. S11 Intermolecular energy of pyrene dimer (s1) calculated by (a) 6-exp potential, and (b) BLYP-D3. Intermolecular energy of perylene dimer (s1) calculated by (c) 6-exp potential, and (d) BLYP-D3. The red circles indicate the calculated minima.

Geometry of s2 is obtained in analogy with eqn (4),

$$Y_{s2} = (b - 2y_0)\cos\frac{\theta}{2} - 2x_0\sin\frac{\theta}{2} \quad \text{(S12)}$$

$$Z_{s2} = (b - 2y_0)\cos\frac{\theta}{2} + 2x_0\sin\frac{\theta}{2} \quad \text{(S13)}$$

where x_0 and y_0 are the coordinates of the s1 molecule in the original rectangular coordinates. When θ ~ 90°, however, Z_{s2} is given by Z_0 = 3.4 Å.

Contributions of dispersion and electrostatic contributions

When dispersion and electrostatic contributions are estimated independently for stacked molecules in Fig. 3(c), 3(d), S8(a), and S11(a), the dispersion term V_{vdW} (eqn (2)) has a minimum at (X_s, Y_s) = (0.0, 0.0), whereas the electrostatic term V_{stat} (eqn (3)) has a repulsive (positive) peak at (0.0, 0.0) (Fig. S12 and S13). As a result, the minimum of the sum V_t appears 1.4-1.8 Å apart from the center. Usually, a staggered overlap is more stable than the eclipsed overlap, but in the present formulation this is derived from the competition of these two terms. In general, V_{vdW} is simply attractive for stacked molecules, while V_{stat} is repulsive because the carbon atoms have slight negative charges. For stacks, the electrostatic contribution makes the slightly slipped molecular arrangement most stable.

For molecules related to the glide plane in analogy with Fig. 3(a) and 3(b), V_{vdW} has a minimum around Y_g = 0.0 Å, but V_{stat} prefers negative Y_g (Fig. S14), and the minimum of the total V_t appears around Y_g = −0.8 Å. Here, the hydrogen atoms of the top molecule come to the center so that the C−H attraction is maximized. This is in agreement with the observe Y_g values in Table 1.

When independent terms are estimated for potential curves in Fig. 5, $V_{t\,vdW}$ is a rather flat curve that does not have a clear minimum around $\theta = 60^o$ (Fig. S15). However, $V_{s\,stat}$ is definitely repulsive (positive) near the stacking structure at $\theta = 180^o$ and slightly attractive (negative) around $\theta = 60^o$. As a result, V_t has a minimum around $\theta = 60^o$. In such thiophene containing molecules as TTT and TTTTT, the contribution of V_{stat} is small due to the absence of the peripheral hydrogen (Table S1). Accordingly, the θ-structure becomes gradually stable. In pentacene and BTBT, $V_{t\,vdW}$ has a minimum near $\theta = 180^o$, and if the atom charges are zero, the stacking or θ-structure is most stable. The V_{stat} term represents preference to the T-type molecular arrangement. This is the reason that the stability of the T-type arrangement is usually explained in terms of the electrostatic attraction.[7-9,24]

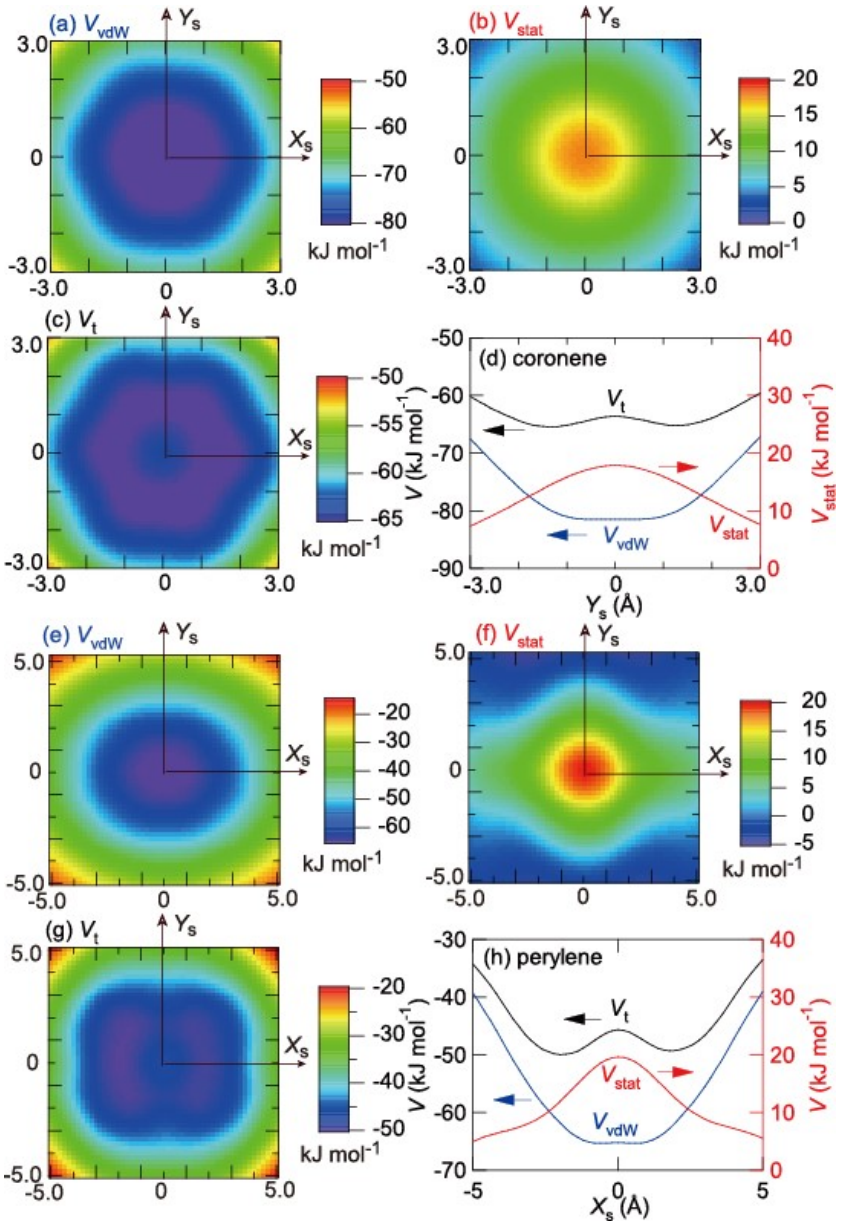

Fig. S12 (a) V_{vdW}, (2) V_{stat}, and (c) the total energy $V_t = V_{vdW} + V_{stat}$ of stacked coronene molecules at Z_s = 3.45 Å, and (d) the intersect at X_s = 0.0 Å. (e) V_{vdW}, (f) V_{stat}, and (g) the total energy $V_t = V_{vdW} + V_{stat}$ of stacked perylene molecules at Z_s = 3.45 Å, and (h) the intersect at X_s = 0.0 Å.

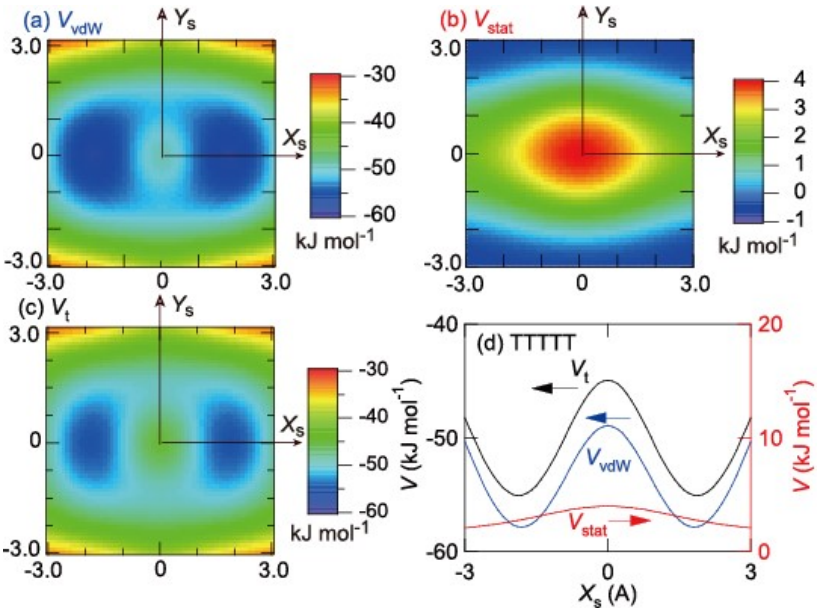

Fig. S13 (a) V_{vdW}, (b) V_{stat}, and (c) the total energy $V_t = V_{vdW} + V_{stat}$ of stacked TTTTT molecules at Z_s = 3.45 Å, and (d) the intersect at Y_s = 0.0 Å.

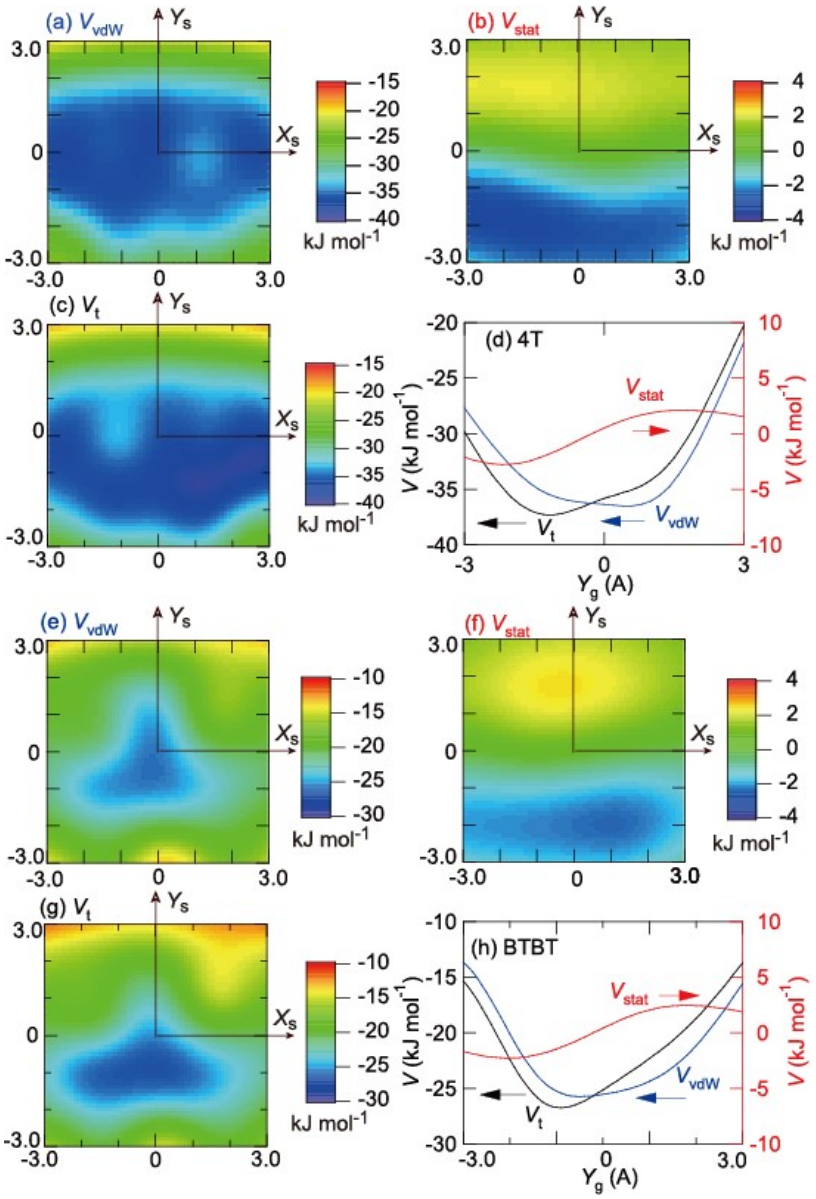

Fig. S14 (a) V_{vdW}, (b) V_{stat}, and (c) the total energy $V_t = V_{vdW} + V_{stat}$ of glide 4T molecules at $Z_g = 4.70$ Å, and (d) the intersect at $X_g = 0.0$ Å. (e) V_{vdW}, (f) V_{stat}, and (g) the total energy $V_t = V_{vdW} + V_{stat}$ of glide BTBT molecules at $Z_g = 4.88$ Å, and (h) the intersect at $X_g = 0.0$ Å.

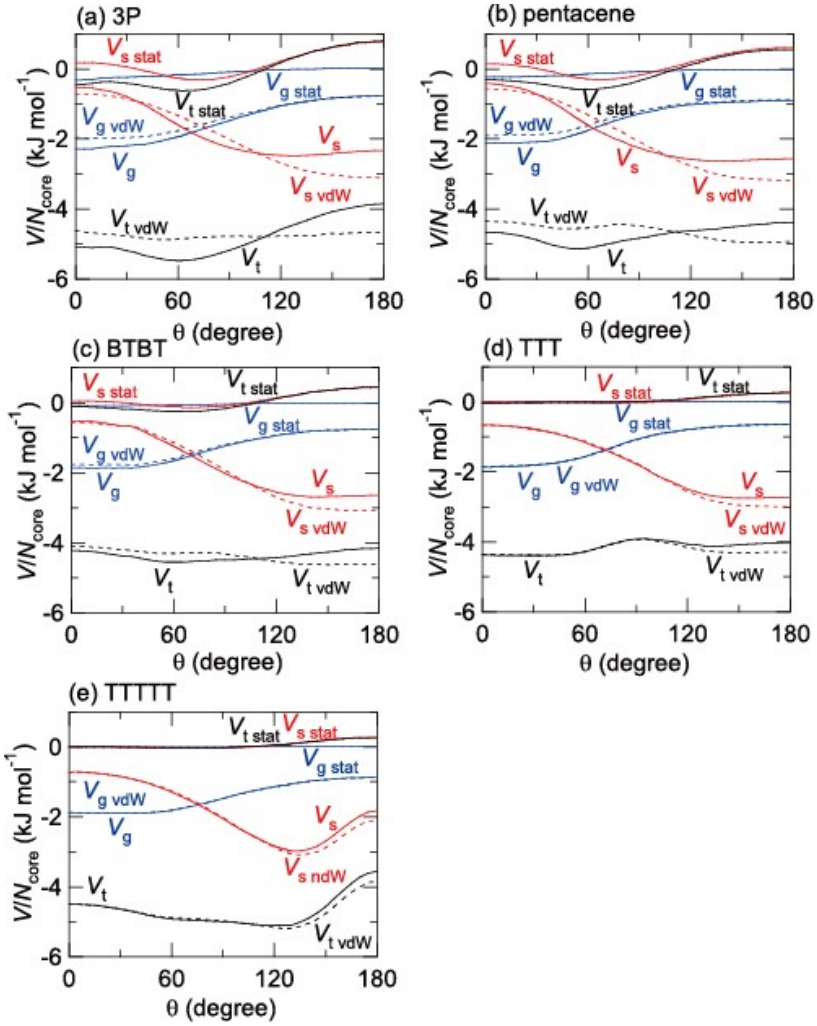

Fig. S15 Independent potential curves for V_{vdW}, V_{stat}, and V_t in (a) 3P, (b) pentacene, (c) BTBT, (d) TTT, and (e) TTTTT.

References

S1 A. Gavezzotti, *Acc. Chem. Res*., 1994, **27**, 309.

S2 M. Mirsky, *Acta Crystallogr. A*, 1976, **32**, 199.

S3 D. E. Williams and T. L. Starr, *Computers Chem*., 1977, **1**, 173.

S4 S. R. Cox, L.-Y. Hsu and D. E. Williams, *Acta Crystallogr. A*, 1981, **37**, 293.

S5 D. E. Williams and S. R. Cox, *Acta Crystallogr., Sect. B: Struct. Crystallogr. Cryst. Chem.*, 1984, **40**, 404.

S6 W. L. Jorgensen and J. Tirado-Rives, *J. Am. Chem. Soc*., 1988, **110**, 1657.

S7 J. R. Holden, Z. Du and H. L. Ammon, *J. Comp. Chem*., 1993, **14**, 422.

S8 W. D. Cornell, P. Cieplak, C. I. Bayly, I. R. Gould, K. M. Merz, Jr., D. M. Ferguson, D. C. Spellmeyer, T. Fox, J. W. Caldwell and P. A. Kollman, *J. Am. Chem. Soc*., 1995, **117**, 5179.

S9 The software is available from http://www.op.titech.ac.jp/lab/mori/lib/exp.html (accessed 2 October 2023).

S10 https://dasher.wustl.edu/tinker/distribution/params/ (accessed 2 October 2023).

S11 J. Iball, S. N. Scrimgeour and D. W. Young, *Acta Crystallogr., Sect. B: Struct. Crystallogr. Cryst. Chem.*, 1976, **32**, 328.

S12 C. C. Mattheus, G. A. de Wijs, R. A. de Groot and T. T. M. Palstra, *J. Am. Chem. Soc*., 2003, **125**, 6323.

S13 C. C. Mattheus, A. B. Dros, J. Baas, A. Meetsma, J. L. DeBoer and T. T. M. Palstra, *Acta Crystallogr., Sect. C.*, 2001, **57**, 939.

S14 S. Schiefer, M. Huth, A. Dobrinevski and B. Nickel, *J. Am. Chem. Soc.*, 2007, **129**, 10316.

S15 K. V. Zaitsev, A. V. Churakov and S. S. Karlov CCDC 1441400: *Exp. Cryst. Struct. Det*., 2015.

S16 S. Grimme, *WIREs Comput. Mol. Sci*., 2011, **1**, 211.

S17 ADF2017.109; Scientific Computing & Modeling (SCM), Theoretical Chemistry, Vrije Universiteit, Amsterdam, The Netherlands, https://www.scm.com (accessed 2 October 2023).